A Sec14p-nodulin domain phosphatidylinositol transfer protein polarizes membrane growth of *Arabidopsis thaliana* root hairs

Patrick Vincent,[1] Michael Chua,[2] Fabien Nogue,[3] Ashley Fairbrother,[1] Hal Mekeel,[1] Yue Xu,[4] Nina Allen,[4] Tatiana N. Bibikova,[5] Simon Gilroy,[5] and Vytas A. Bankaitis[1]

[1]Department of Cell and Developmental Biology and [2]Department of Cell and Molecular Physiology, Michael Hooker Microscopy Facility, University of North Carolina School of Medicine, Chapel Hill, NC 27599
[3]Station de Génétique et d'Amélioration des Plantes, Institut National de la Recherche Agronomique, 78026 Versailles-Grignon, France
[4]Department of Botany, North Carolina State University, Raleigh, NC 27695
[5]Department of Biology, The Pennsylvania State University, University Park, PA 16802

Phosphatidylinositol (PtdIns) transfer proteins (PITPs) regulate signaling interfaces between lipid metabolism and membrane trafficking. Herein, we demonstrate that AtSfh1p, a member of a large and uncharacterized *Arabidopsis thaliana* Sec14p-nodulin domain family, is a PITP that regulates a specific stage in root hair development. AtSfh1p localizes along the root hair plasma membrane and is enriched in discrete plasma membrane domains and in the root hair tip cytoplasm. This localization pattern recapitulates that visualized for PtdIns(4,5)P_2 in developing root hairs. Gene ablation experiments show AtSfh1p nullizygosity compromises polarized root hair expansion in a manner that coincides with loss of tip-directed PtdIns(4,5)P_2, dispersal of secretory vesicles from the tip cytoplasm, loss of the tip f-actin network, and manifest disorganization of the root hair microtubule cytoskeleton. Derangement of tip-directed Ca^{2+} gradients is also apparent and results from isotropic influx of Ca^{2+} from the extracellular milieu. We propose AtSfh1p regulates intracellular and plasma membrane phosphoinositide polarity landmarks that focus membrane trafficking, Ca^{2+} signaling, and cytoskeleton functions to the growing root hair apex. We further suggest that Sec14p-nodulin domain proteins represent a family of regulators of polarized membrane growth in plants.

Introduction

Sec14p, the major yeast phosphatidylinositol (PtdIns) transfer protein (PITP), regulates an essential interface between lipid metabolism and protein transport from Golgi membranes to the cell surface (Bankaitis et al., 1990; Cleves et al., 1991a,b; Xie et al., 1998). This regulatory circuit, termed the Sec14p pathway, defines a signaling cascade that involves functionally uncharacterized proteins of the oxysterol binding protein family such as Kes1p (Fang et al., 1996; Li et al., 2002) and ADP-ribosylation factor GTPase activating proteins (Yanagisawa et al., 2002). These regulatory interactions couple lipid signaling to the function of core components of the vesicle trafficking machinery, but precisely how this occurs remains unknown.

Mammals express at least three soluble PITPs: PITPα, PITPβ, and rdgBβ; and all of these share primary sequence homology to each other (for review see Routt and Bankaitis, 2004). The mammalian PITP module is found throughout metazoans and is structurally unrelated to yeast PITPs (Sha et al., 1998; Yoder et al., 2001). Gene ablation experiments in mice, although suggesting an essential housekeeping function for PITPβ, demonstrate that PITPα nullizygosity results in chylomicron retention disorder, severe hypoglycemia, and a fulminating spinocerebellar neurodegenerative disease (Alb et al., 2002, 2003). As at least some forms of human chylomicron retention disease are caused by null mutations in the Sar1b GTPase that regulates coassembly of COPII coat components with ER cargo (Jones et al., 2003), PITPα is suggested to regulate a Sar1b-GTPase activating protein function on the enterocyte ER

Correspondence to Vytas A. Bankaitis: vytas@med.unc.edu; or Patrick Vincent: patrick_vincent@med.unc.edu

Abbreviations used in this paper: ESEM, environmental scanning EM; GUS, β-glucuronidase; LBD, lipid binding domain; MT, microtubule; PH, pleckstrin homology; PIP, phosphoinositide; PITP, PtdIns transfer protein; PLCδ1, phospholipase Cδ1; PLD, phospholipase D; PtdCho, phosphatidylcholine; PtdIns, phosphatidylinositol; PtdOH, phosphatidic acid; SIET, scanning ion-selective electrode technique; VRZ, vesicle-rich zone.

The online version of this article includes supplemental material.

The Journal of Cell Biology, Vol. 168, No. 5, February 28, 2005 801–812
http://www.jcb.org/cgi/doi/10.1083/jcb.200412074

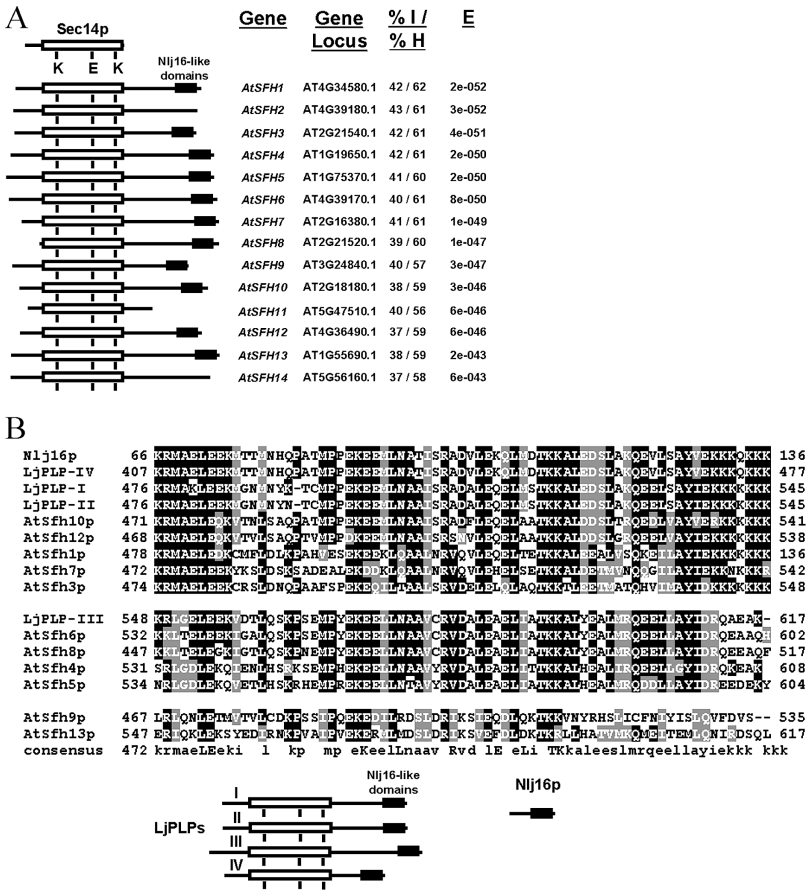

Figure 1. **The *A. thaliana* Sec14p-nodulin domain family.** (A) Schematic alignment of Sec14p with *AtSFH* gene products (identified by TAIR accession numbers). Primary sequence identities/homologies with Sec14p are indicated. Probabilities that these relationships are random are given (E-values). The indicated K_{66}, E_{207}, and K_{239} residues critical for Sec14p binding of phosphatidylinositol are highly conserved (Phillips et al., 1999). (B) Primary sequence alignment of the COOH-terminal 70 *AtSFH* nodulin domain residues with those of the Nlj16 nodulin (Szczyglowski et al., 1997). Conserved identities and similarities are highlighted. Schematic illustration of the domain organization of four members of this family from the legume *Lotus japonicus* is also shown. These LjPLPs exhibit COOH-terminal Nlj16 nodulin domains.

surface in the chylomicron biogenic pathway (Bankaitis et al., 2004). Indeed, the hypothesis for PITPα function in chylomicron trafficking shares basic features with that proposed for Sec14p function in yeast (Yanagisawa et al., 2002) and leaves open the possibility that structurally disparate PITPs nonetheless operate via similar mechanisms in regulating analogous membrane trafficking reactions.

Although PITPs exist in higher plants (Jouannic et al., 1998; Kearns et al., 1998a), there has been no systematic functional analysis of them. Herein, we describe a large and novel family of Sec14p-nodulin domain proteins in *Arabidopsis thaliana*. We show that the Sec14p domains of these proteins share functional properties consistent with those of Sec14p-like PITPs and report the first analysis of the biological function of any Sec14p-like protein in plants. We demonstrate that loss of AtSfh1p, a membrane-bound Sec14p-nodulin protein, dramatically compromises polarized root hair membrane trafficking. Derangement of polarized membrane growth occurs after the site of root hair emergence has been correctly determined and emergence initiated. The collective data suggest AtSfh1p generates phosphoinositide (PIP) landmarks that focus membrane delivery to the root hair tip plasma membrane in a manner that depends on the actin cytoskeleton. The results further suggest that the polarized secretory pathway establishes a tip-directed Ca^{2+} gradient that cues microtubule (MT) organization in a manner that further reinforces tip-directed membrane trafficking. The collective data describe the functional characterization of the role for a novel membrane-associated PITP in execution of developmentally regulated polarized membrane trafficking pathway.

Results

A novel family of Sec14p-nodulin domain proteins

A search of the National Center for Biotechnology Information and The Arabidopsis Information Resource databases identified 31 homologous *A. thaliana* sequences when the Sec14p primary sequence was queried. These sequences each exhibit a 239-residue domain that shares significant primary sequence homology with the Sec14p lipid binding domain (LBD), and these domains fall into two Sec14p homology groups. One Sec14p homology group encodes proteins that consist of a Sec14p domain that shares rather low (but significant) sequence identity with yeast Sec14p. The other Sec14p homology group consists of the 14 highest-scoring Sec14p LBD-like sequences. 11 of these 14 sequences represent proteins where an NH_2-terminal Sec14p domain is joined to a COOH-terminal nodulin domain of ~100 residues (Fig. 1 A). These nodulin domains define three classes based on similarity to the Nlj16 nodulin (Fig. 1 B). Nlj16 is expressed by root cells of the legume *Lotus japonicus* upon infection with *Rhizobium* and defines a plasma membrane targeting module (Kapranov et al., 2001). *Lotus* expresses four Sec14p-nodulin domain genes (LjPLP-I

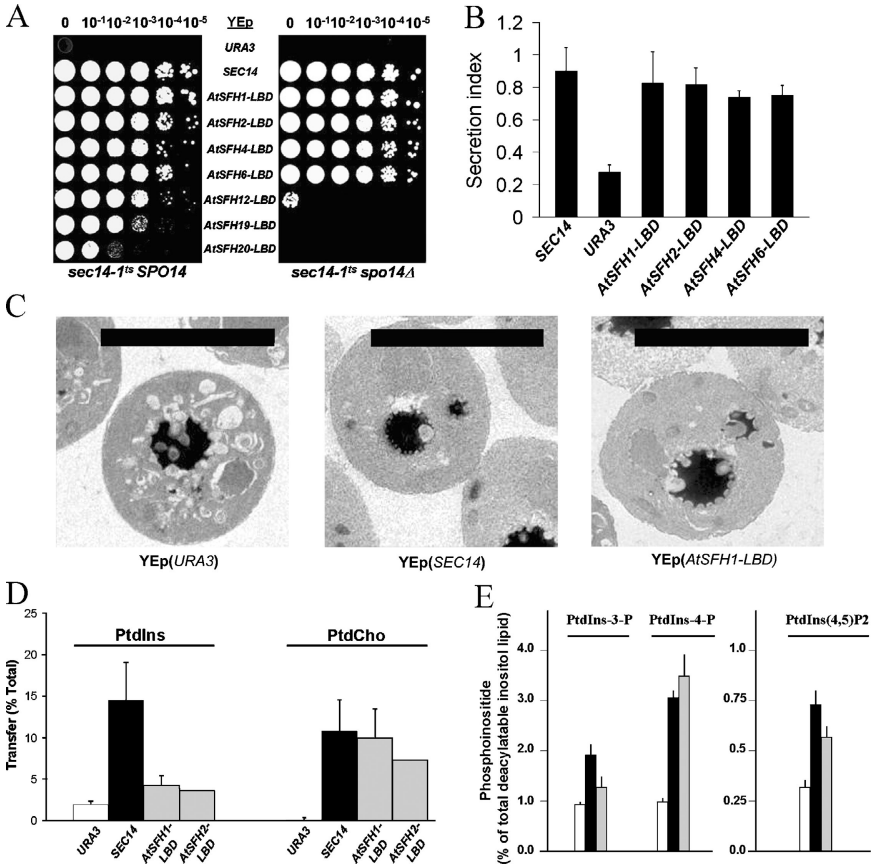

Figure 2. **Sec14p-like LBDs exhibit intrinsic PITP activities.** (A) Isogenic *sec14-1*^{ts} and *sec14-1*^{ts} spo14Δ yeast strains carrying the indicated YEp plasmids were spotted in 10-fold dilution series onto agar plates and incubated at the restrictive temperature of 37°C. YEp(*URA3*) and YEp(*SEC14*) derivatives served as negative and positive controls. (B) Invertase secretion indices (secreted invertase/total invertase) are shown for *sec14-1*^{ts} strains carrying the designated YEp plasmids at 37°C. YEp(*URA3*) and YEp(*SEC14*) derivatives served as negative and positive controls. (C) Electron micrographs of *sec14-1*^{ts} yeast strains carrying the designated YEp plasmids after 37°C challenge for 2 h. Bars = 5 μm. (D) PtdCho- (right; $n = 3$) and PtdIns-transfer assays ($n = 7$; Li et al., 2000). Cytosols prepared from the *sec14*Δ yeast strain CTY303 harboring the YEp(*URA3*) negative control, the YEp(*SEC14*) positive control, YEp(*AtSFH1-LBD*), and YEp(*AtSFH2-LBD*) were assayed, as indicated. The PtdIns- and PtdCho-transfer assays used 2 and 1 mg of cytosol, respectively. (E) PIP analyses. Isogenic derivatives of the *sec14*Δ yeast strain CTY303 carrying designated YEp plasmids were radiolabeled for 18 h at 25°C with 20 μCi/ml [^{3}H]inositol. PIPs were extracted, deacylated, and quantified. PtdIns-3-phosphate, PtdIns-4-phosphate, and PtdIns(4,5)P_2 are as indicated; $n = 6$. YEp(*URA3*) and YEp(*SEC14*) derivatives served as negative and positive controls (white bars and black bars, respectively), whereas the YEp(*AtSFH1-LBD*) values are in gray bars. All PIP levels were increased in YEp(*SEC14*) and YEp(*AtSFH1-LBD*) derivative strains relative to the YEp(*URA3*) negative control ($P < 0.001$).

thru LjPLP-IV; Fig. 1 B). The Sec14p-nodulin domain proteins are of special interest because of the unanticipated physical linkage of Sec14p and nodulin domains, and because these define unique examples of membrane-bound Sec14p-like PITPs.

AtSfhp-LBDs and Sec14p share functional properties

Expression in yeast of AtSfh1p-, AtSfh2p-, AtSfh4p-, or AtSfh6p-LBDs rescued growth defects associated with *sec14-1*^{ts} (Fig. 2 A) and haploid-lethal *sec14*Δ alleles (not depicted). These results were scored in phospholipase D (PLD)–proficient (*SPO14*) or –deficient (*spo14*Δ) genetic backgrounds. PLD deficiencies exacerbate Sec14p defects, and assessment of rescue in both *SPO14* and *spo14*Δ genetic backgrounds reports quality of rescue. As an example, expression of *AtSFH19* (AT5G47730.1) or *AtSFH20* (AT1G01630.1) (i.e., representatives of the second Sec14p homology group) rescued *sec14-1*^{ts} alleles in *SPO14* but not *spo14*Δ yeast strains (Fig. 2 A). Rescue of *sec14* growth defects by AtSfh1p-, AtSfh2p-, AtSfh4p-, or AtSfh6p-LBDs extended to restoration of invertase secretion from Sec14p-deficient Golgi membranes (Fig. 2 B) and normal morphology to Sec14p-deficient cells (Fig. 2 C). The toroid structures observed in *sec14-1*^{ts} cells incubated at restrictive temperature represent defective Golgi compartments engorged with secretory cargo. AtSfh1p-LBD expression restores wild-type morphology to >90% of *sec14-1*^{ts} cells (Fig. 2 C).

AtSfhp-LBDs exhibit intrinsic PITP biochemical activities. AtSfh1p- and AtSfh2p-LBDs catalyzed phosphatidylcholine (PtdCho)- and PtdIns-transfer in vitro (Fig. 2 D). Significance of the PtdIns-transfer activities of AtSfh1p- and AtSfh2p-LBD was confirmed in measurements of PIP synthesis in a Sec14p-deficient yeast strain with basal PIP levels that expressed each LBD. In these experiments, the appropriate yeast strains were radiolabeled to steady-state with *myo*-[2-^{3}H] inositol. Bulk PIPs were extracted, deacylated to yield the corresponding glycerophosphoinositol derivatives of extracted PIP species, and the water-soluble glycerophosphoinositols were chromatographically resolved and quantified (see Materials and methods). AtSfh1p-LBD expression elicited significant elevations in steady-state PtdIns-3-phosphate, PtdIns-4-phosphate, and PtdIns-4,5-P_2 levels in the yeast tester strain compared with mock control (Fig. 2 E). These elevations in bulk PtdIns-4-phosphate and PtdIns-4,5-P_2 content were of the magnitude recorded for the YEp(*SEC14*) positive control. AtSfh2p-LBD expression also elevated bulk PIP levels (unpublished data).

AtSFH1 function is required for proper root hair elongation

Sec14p-nodulin domain proteins are uncharacterized and expansion of this family suggests tissue-specific functions for its members. AtSfh1p was chosen for detailed analysis because the AtSfh1p-LBD is most homologous to Sec14p. RT-PCR analyses indicated essentially root-specific expression of *AtSFH1* (unpublished data), a result in accord with microarray data (http://www.cbs.umn.edu/arabidopsis/). β-Glucuronidase (GUS) histochemical staining confirmed and extended these re-

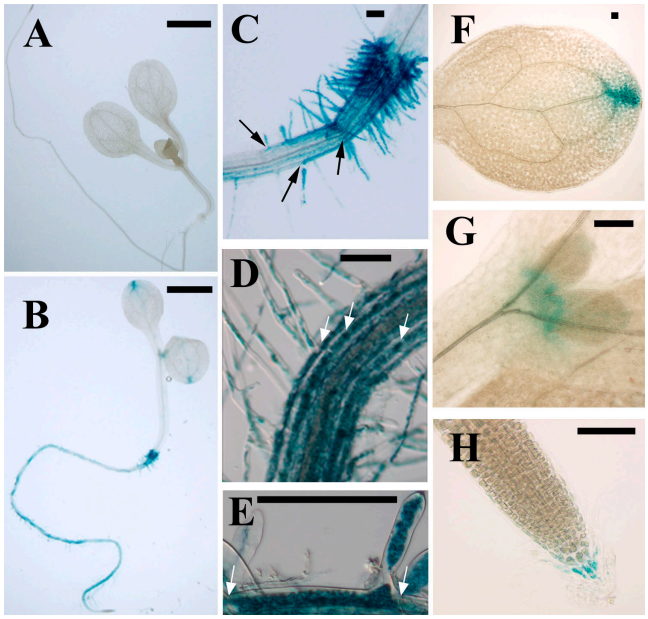

Figure 3. **Tissue-specific AtSfh1p expression.** Otherwise wild-type transgenic plants stained for GUS expressed from a promoterless construct (A) or the *AtSFH1* promoter (P_{AtSFH1}::GUS) (B). (C) P_{AtSFH1}::GUS expression is robust in root. Arrows denote GUS-active trichoblast cell files. (D) Root hair producing epidermal cell files (arrows) exhibit robust P_{AtSFH1}::GUS expression. (E) GUS activity is recorded both in trichoblast cell bodies and root hairs. Arrows denote cell plates. P_{AtSFH1}::GUS activity in cotyledon hydathodes (F), apical shoot meristem (G), and apical cells of the root cap (H). Bars: (A and B) 0.12 cm; (C–H) 50 μm.

sults. *AtSFH1* was expressed solely in root trichoblast cell files engaged in root hair growth (Fig. 3, C–E), hydathodes, shoot apical meristem, and apical cells of the root cap (Fig. 3, F–H).

Atsfh1::T-DNA plants (Fig. 4 A) were substantially normal and fertile. However, mutant plants elaborated short root hairs. Mutant single root hairs from 3-d-old seedlings were one-third the length of age-matched wild-type structures (69 ± 13 vs. 224 ± 51 μm, $n = 55$) and exhibited half the surface area (3494 ± 902 vs. 6924 ± 1045 μm^2, $n = 55$). Mutant and wild-type single root hairs exhibited similar volumes (14866 ± 5550 vs. 17113 ± 3510 μm^3, $n = 55$), as did double root hairs (unpublished data). These disparities persisted throughout the lifetime of the plant (Fig. 4 B). In addition, *Atsfh1::T-DNA* root hairs appeared flaccid. This observation was in contrast to the rigid profiles exhibited by age-matched wild-type root hairs (Fig. 4 C). Although there is robust *AtSFH1* expression in apical cells of the root cap, *Atsfh1::T-DNA* primary roots exhibit no defects in gravitropism (unpublished data).

Reduced lengths of *Atsfh1::T-DNA* root hairs reflect failures in polarized membrane growth. High frequencies of *Atsfh1::T-DNA* root hairs with two growing tips were observed and a significant number exhibited three. Wild-type plants rarely elaborated two growing tips, and we never observed any with three (Fig. 4, C and D). Double root hairs exhibited volumes similar to those of wild-type root hairs, but only 50% of the surface area. The data indicate AtSfh1p-deficient root hairs exhibit impaired secretion efficiency and failure in restricting active growing points to a single site that leads to isotropic root hair cell expansion. Yet, *Atsfh1::T-DNA* plants correctly specified site of root hair emergence from the distal plasma membrane of parent epidermal cells (Fig. 4 E). Moreover, consistent with the tissue restriction of *AtSFH1* expression, nullizygous plants did not exhibit obvious defects in other organs (such as leaf trichomes and pollen tubes) whose development requires polarized membrane trafficking (unpublished data).

Four lines of evidence demonstrate the full spectrum of *Atsfh1::T-DNA* root hair phenotypes results from a single fully penetrant recessive mutation. First, cross of *Atsfh1::T-DNA* homozygotes to wild-type plants yielded only wild-type progeny. Second, the root hair phenotype cosegregated with *Atsfh1::T-DNA* through multiple (>3) backcrosses. Third, transgenic *Atsfh1::T-DNA* plants bearing ectopic *AtSFH1* exhibited normal root hairs (Fig. 4 F). Four, examination of 2947 F2 progeny from three independent *Atsfh1::T-DNA/Atsfh1::T-DNA* X *AtSFH1/AtSFH1* crosses yielded 701 mutant (23.8%) and 2,246 (76.2%) wild-type phenotypes, respectively. To assess the functional importance of the Sec14p domain, we generated an NH_2-terminal GFP-fusion to the AtSfh1p-LBD that inactivates Sec14p domain activities. GFP-AtSfh1p, when placed in the context of full-length AtSfh1p and expressed in plants, fails to complement *Atsfh1::T-DNA* (Fig. 4 F). Similarly, a COOH-terminal GFP-fusion that preserves Sec14p domain function, but abuts the nodulin domain, also fails to complement *Atsfh1::T-DNA* (unpublished data). Thus, both functional Sec14p and nodulin domains are critical for AtSfh1p function in plants.

Localization of AtSfh1p in developing root hairs

The AtSfh1p nodulin domain exhibits high primary sequence identity to the Nlj16 nodulin. As Nlj16 functions as a plasma membrane targeting domain (Kapranov et al., 2001), we expected AtSfh1p would also localize to membranes. Consistent with expectation, the GFP-AtSfh1p chimera (with the caveat that it harbors a nonfunctional Sec14p domain) distributed in an apex-directed spiraling arrangement along the root hair cortical plasma membrane in otherwise wild-type plants (Fig. 5 A, top left; and Video 1, available at http://www.jcb.org/cgi/content/full/jcb.200412074/DC1). Optical cross sections taken through the root hair at positions removed from the apex also indicated a plasma membrane localization for GFP-AtSfh1p (Fig. 5 A, top right). Optical sectioning of the apex plasma membrane at the root hair tip reported a clear enrichment of GFP-AtSfh1p staining on the plasma membrane at that site as well (Fig. 5 A, bottom panel). That this profile reflects plasma membrane staining was confirmed in FM1-43 double label experiments. Under conditions where FM1-43 selectively labels plasma membrane, FM1-43 and GFP-AtSfh1p staining were coincident (unpublished data). Strong enhancement of GFP-AtSfh1p reporter fluorescence was also recorded in the tip cytoplasm (Fig. 5 A, top left and bottom panel; and Video 1). For the reasons detailed in the section Ultrastructure of the *Atsfh1* tip cytoplasm, we interpret this staining to reflect an AtSfh1p pool that is localized on post-Golgi vesicles. Expression of GFP or YFP alone gave diffuse staining (Figs. S1 and S2, available at http://www.jcb.org/cgi/content/full/jcb.200412074/DC1).

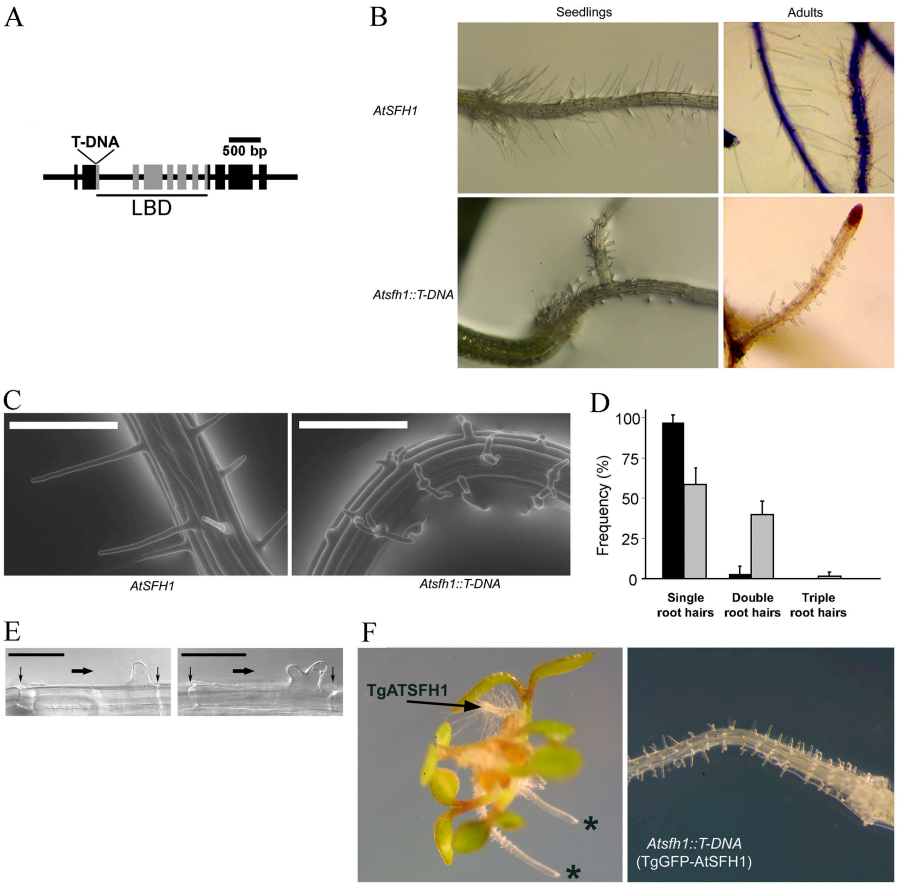

Figure 4. **AtSfh1p function is essential for proper root hair development.** (A) Genomic structure of *AtSFH1*. Sites of T-DNA insertion and the LBD coding regions are indicated. The *Atsfh1::T-DNA* allele harbors three T-DNA copies at the single site of insertion. (B) Root hair profiles of wild-type (top) and *Atsfh1::T-DNA* (bottom) plants. Corresponding profiles of 3-d-old seedlings (left) and adult plants (right) are shown. (C) ESEM of living 3-d-old wild-type (left) and *Atsfh1::T-DNA* (right) seedlings. Bars, 200 μm. (D) Frequencies of single, double, and triple root hairs in 3-d-old wild-type (black bars) and *Atsfh1::T-DNA* (gray bars) seedlings as determined by ESEM of 250 root hairs of each genotype (25 root hairs from each of 10 seedlings). Frequencies of each class of root hair morphology were determined for each individual seedling and the average frequencies and standard errors are given. (E) Nomarski images of wild-type (left) and *Atsfh1::T-DNA* (right) root epidermal cells initiating root hair growth. Vertical arrows identify cell plates. Horizontal arrows identify direction of primary root growth. Bars = 50 μm. (F) Root hair profiles of 3-d-old seedlings. (left) *Atsfh1::T-DNA* (*) and transgenic derivative bearing an ectopic wild-type gene (*TgAtSFH1*). (right) Transgenic *Atsfh1::T-DNA* seedling expressing an NH_2-terminal (*TgGFP-AtSFH1*) gene fusion.

PtdIns(4,5)P_2 deficiencies in *Atsfh1* root hairs

The ability of AtSfh1p-LBD to stimulate PIP synthesis suggests AtSfh1p mediates PIP-dependent regulation of polarized membrane transport in *A. thaliana*. Because polarized membrane transport in yeast and plants requires involvement of the actin cytoskeleton and actin dynamics are responsive to PtdIns(4,5)P_2, we focused on the role of AtSfh1p in modulating PtdIns(4,5)P_2 homeostasis. Using a phospholipase Cδ1 (PLCδ1) pleckstrin homology (PH) domain–YFP reporter to infer PtdIns(4,5)P_2 status, we found wild-type root hairs exhibited a tip-directed (4,5)P_2 gradient on the root hair plasma membrane. Indeed, PtdIns(4,5)P_2 was distributed in a pattern similar to that recorded for GFP-AtSfh1p in wild-type root hairs. Discrete PtdIns(4,5)P_2–enriched domains were also recorded along the cortical root hair plasma membrane (Fig. 5 B, top left). Pseudocolor rendering of $PH_{PLC\delta1}$–YFP fluorescence revealed a tip-directed spiraling arrangement along the cortical root hair plasma membrane (Fig. 5 B, top right and bottom left; and Video 2, available at http://www.jcb.org/cgi/content/full/jcb.200412074/DC1), and optical sectioning of the tip plasma membrane revealed a high concentration of PtdIns(4,5)P_2 at the very apex of the root hair (Fig. 5 B, bottom right). Again, FM1-43 double-labeling experiments confirmed the plasma membrane localization of the $PH_{PLC\delta1}$–YFP reporter fluorescence (see the following paragraph). Strikingly, as was observed for AtSfh1p-GFP, optical cross sections of the root hair apex demonstrated strong enhancement of $PH_{PLC\delta1}$–YFP reporter fluorescence in the tip cytoplasm.

Given the ability of AtSfh1p-LBD to stimulate PIP synthesis, we anticipated *Atsfh1::T-DNA* root hairs would exhibit PIP deficiencies. We focused on PtdIns(4,5)P_2 as this phospholipid is an established regulator of polarized membrane trafficking. Indeed, the tip-directed PtdIns(4,5)P_2 gradient was compromised, and the prominent cytoplasmic $PH_{PLC\delta1}$–YFP reporter fluorescence was absent from mutant tip cytoplasm (Fig. 5, C and D; and Videos 3 and 4, available at http://www.jcb.org/cgi/content/full/jcb.200412074/DC1). That PtdIns(4,5)P_2 is enriched at the tip plasma membrane of wild-type root hairs, and that this PtdIns(4,5)P_2 enrichment is lost in mutant tip plasma membrane, was indicated by ratiometric imaging of $PH_{PLC\delta1}$–YFP/FM1-43 fluorescence in double-label experiments. From those experiments, we record a threefold tip enrichment of PtdIns(4,5) P_2 in wild-type root hair tip plasma membrane relative to cortical plasma membrane. We detected loss of PtdIns(4,5)P_2 tip enrichment in the *Atsfh1* tip plasma membrane relative to wild-type and estimate a 5–10-fold reduction in relative PtdIns(4,5) P_2 in mutant tip plasma membrane (Fig. 5 E). No obvious PtdIns(4,5) P_2 deficiencies were recorded in the cortical plasma membrane of *Atsfh1::T-DNA* root hairs.

Ultrastructure of the *Atsfh1* tip cytoplasm

Loss of $PH_{PLC\delta1}$–YFP fluorescence staining in the tip cytoplasm of AtSfh1p-deficient root hairs was a striking phenotype. Because incubation of metabolically active wild-type root hairs

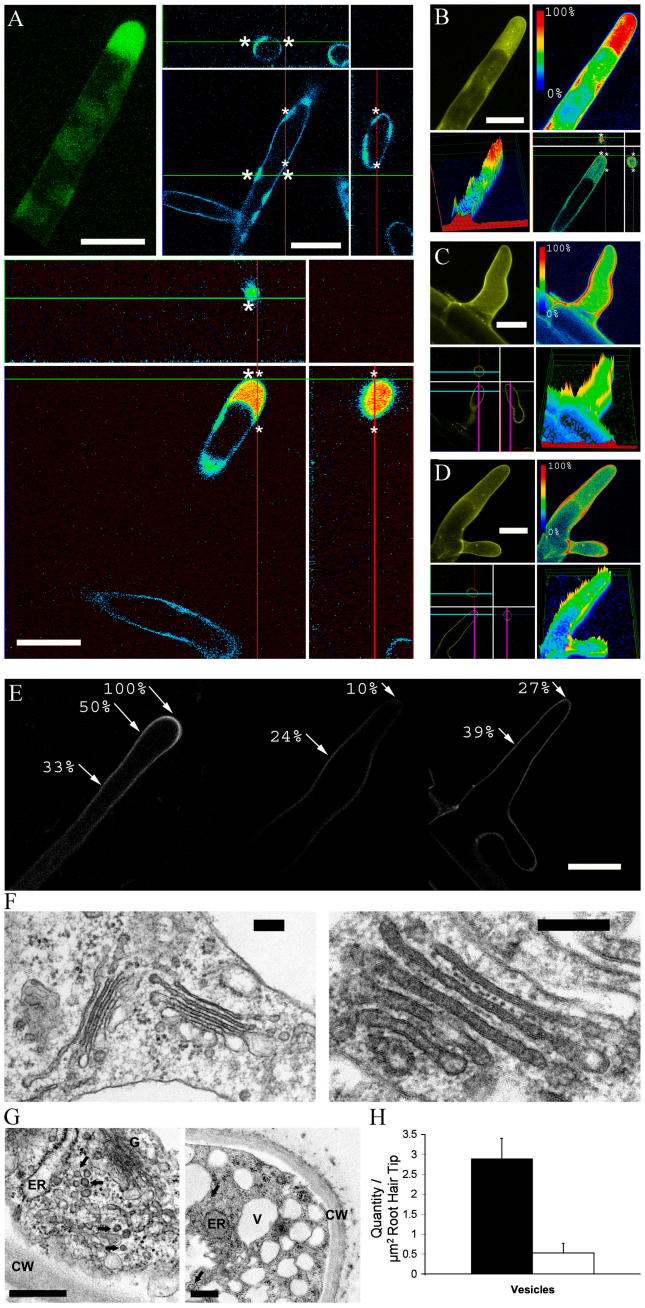

Figure 5. **Deranged signaling in AtSfh1p-deficient root hairs.** (A) AtSfh1p localization in developing root hairs. Focal planes of optical cross sections are indicated by corresponding colored lines. Large and small asterisks indicate corresponding positions in cross section. GFP was fused to the AtSfh1p NH_2 terminus. (B–D) PtdIns(4,5)P_2 distribution in 3-d-old wild-type (B) and *Atsfh1::T-DNA* single (C) and double (D) root hairs. Panels for each image set (left to right from top): $PH_{PLC\delta1}$–YFP fluorescence, relative intensities of $PH_{PLC\delta1}$–YFP fluorescence in pseudocolor according to the inset scale (arbitrary intensity units), landscape pseudocolor profile of fluorescence throughout imaged root hair, and $PH_{PLC\delta1}$–YFP fluorescence in a single cross section of hair tips (focal plane of section indicated by colored lines). Large and small asterisks indicate corresponding positions in cross section. In all panels other than those denoting specific cross sections, 100 serial confocal sections were collapsed and summed to generate each image. Expression of YFP alone yielded uniform fluorescence throughout the root hair cytoplasm (see online supplemental materials). (E) Ratiometric imaging of $PH_{PLC\delta1}$–YFP/FM1-43 fluorescence. 3-d-old wild-type seedlings expressing $PH_{PLC\delta1}$–YFP were incubated and labeled with FM1-43 under conditions that selectively label the plasma membrane. $PH_{PLC\delta1}$–YFP and FM1-43 images were collected immediately and merged. The fluorescence ratio was measured at points indicated by arrows. $PH_{PLC\delta1}$–YFP/FM1-43 fluorescence in wild-type root hair apex was set as 100% and all other ratios indicated are normalized to this value. (F) EM micrographs of representative Golgi compartments in wild-type (left) and *Atsfh1::T-DNA* (right) root hairs. (G) EM micrographs of wild-type (left) and *Atsfh1::T-DNA* VRZ (right). Arrows indicate vesicles. G, Golgi stack; ER, endoplasmic reticulum; V, vacuoles; CW, cell wall. (H) Quantification of membranes in the VRZ. Vesicles (70–100-nm-diam) were counted in EM micrographs of tip cytoplasm from wild-type (closed bar) and mutant (open bar) root hairs from 3-d-old plants. Data were collected from two root hair tips from each of three independent plants of each genotype. Bars: (A–E) 20 μm; (F) 0.2 μm; (G) 0.5 μm.

for 20 min with FM1-43 yielded robust staining of the tip cytoplasm, in a fashion that recapitulated the pattern of GFP-AtSfh1p and $PH_{PLC\delta1}$–YFP tip fluorescence (unpublished data), we interpreted $PH_{PLC\delta1}$–YFP fluorescence in tip cytoplasm to reflect the status of small membrane-enclosed structures in this region. In this regard, tip cytoplasm is enriched for post-Golgi secretory vesicles and is referred to as the vesicle-rich zone (VRZ; Braun et al., 1999). Therefore, we inspected wild-type and mutant root hair apices by electron microscopy. Wild-type and *Atsfh1::T-DNA* Golgi stack ultrastructures were indistinguishable in appearance (Fig. 5 F) and in physical parameters (Table I). The structural integrity of *Atsfh1::T-DNA* Golgi membranes suggested these systems are not grossly defective in secretory function. Golgi stack distribution throughout the cytoplasm was also unaffected in the mutant root hairs (Fig. S3, available at http://www.jcb.org/cgi/content/full/jcb.200412074/DC1). However, two unusual properties of mutant tip cytoplasm were apparent. First, the concentration of vesicles per unit tip cytoplasm was reduced sixfold in mutant relative to wild-type VRZ (Fig. 5, G and H). We interpret this result, and the loss of tip cytoplasm fluorescence as recorded by the GFP-AtSfh1p and $PH_{PLC\delta1}$–YFP reporters (see the section Localization of AtSfh1p in developing root hairs), to indicate a dispersal of vesicles from the VRZ throughout the mutant root hair cytoplasm. Second, dramatic vacuolation of the mutant VRZ and tip cytoplasm was observed (Fig. 5 G).

The tip f-actin cytoskeleton is compromised in *Atsfh1* root hairs

Vacuolation of *Atsfh1::T-DNA* root hair tip cytoplasm recapitulated the effects recorded in root hairs where the actin cytoskeleton was disrupted (Čiamporová et al., 2003). To assess f-actin status in *Atsfh1::T-DNA* root hairs, we used GFP-talin as a reporter for f-actin. These imaging experiments indicated that wild-type root hairs exhibit a discrete cortical actin meshwork and a tip-concentrated f-actin microfilament network in the VRZ (Fig. 6 A and Video 5, available at http://www.jcb.org/cgi/content/full/jcb.200412074/DC1), as described previously (Baluška et al., 2000; Smith, 2003). However, selective defects in the f-actin cytoskeleton were apparent in mutant root hairs. Although the cortical actin cytoskeleton of mutant root hairs remained intact, the tip-directed f-actin microfilament component was lost (Fig. 6, B and C; and Videos 6 and 7, available at http://www.jcb.org/cgi/content/full/jcb.200412074/DC1). As tip f-actin microfilament networks focus transport vesicle de-

Table I. **Physical dimensions of wild-type and *Atsfh1* nullizygous root hair Golgi membranes**

Plant genotype	Cisternal length	Stack width	Cisternal width	Cisternae per stack
	nm	*nm*	*nm*	
AtSFH1	750 ± 154 (22)	290 ± 81 (19)	30 ± 7 (22)	4.7 ± 0.4 (22)
Atsfh1::T-DNA	690 ± 162 (26)	321 ± 85 (24)	34 ± 7 (110)	4.4 ± 0.7 (110)

Cisternal length represents the longest dimension, and width was calculated for each cisterna in the mid-axis of each Golgi stack. Stack width is measured along the cis-trans axis at the midpoint of each stack. Numbers in parentheses represent the number of Golgi stacks analyzed from a total of three independent plants.

livery to the hair apex (Mathur and Hülskamp, 2002; Ketelaar et al., 2003), defects in this actin network are expected to result in dispersal of transport vesicles throughout the root hair cytoplasm. Indeed, loss of the f-actin microfilament network in *Atsfh1::T-DNA* root hairs coincides with loss of $PH_{PLC\delta1}$–YFP fluorescence in the tip cytoplasm.

Isotropic influx of Ca^{2+} into *Atsfh1* root hairs

One critical contributing cue that controls polarized root hair growth is a tip-directed Ca^{2+} gradient. Defects in polarized membrane trafficking are expected to randomize ion (e.g., Ca^{2+}) channel delivery to the plasma membrane, with the consequence that spatial regulation of Ca^{2+} signaling will be compromised. To investigate whether or not dysregulation of Ca^{2+} signaling was occurring in *Atsfh1::T-DNA* root hairs, we used Indo-1 loading strategies to image Ca^{2+} signaling in wild-type and isogenic *Atsfh1::T-DNA* root hairs. Striking derangements in Ca^{2+} signaling to the growing apex of the root hair plasma membrane were observed (Fig. 7 A). Ca^{2+} imaging recorded a single tip-focused Ca^{2+} gradient in wild-type root hairs, as reported previously (Wymer et al., 1997), with tip cytoplasmic Ca^{2+} reaching concentrations in excess of 600 nM. Cytoplasmic Ca^{2+} fell to concentrations below 100 nM very rapidly away from the root hair tip. In marked contrast, precocious Ca^{2+} signaling was evident along the *Atsfh1* root hair cortical plasma membrane with local Ca^{2+} concentrations reaching 600 nM or greater (Fig. 7 A).

One potential mechanism for spatial dysregulation of Ca^{2+} signaling is the isotropic delivery or distribution of active Ca^{2+} channels in the mutant root hair surface. To test this prediction, we used the scanning ion-selective electrode technique (SIET) to monitor Ca^{2+} fluxes along the root hair surface in wild-type and *Atsfh1* nullizygous seedlings (see Materials and methods). Inward Ca^{2+} fluxes exceeding 4 pmol cm^{-2} s^{-1} were recorded around the apex region of growing wild-type root hairs, and Ca^{2+} influx decreased dramatically as the self-referencing probe was positioned away from the root hair apex (Fig. 7, B and C). The flux profiles for *Atsfh1* nullizygous single root hairs were dramatically altered, however. Large inward Ca^{2+} fluxes were not restricted to the tip region. Rather, robust fluxes exceeding 4 pmol cm^{-2} s^{-1} were detected all along the root hair surface. These flux profiles are completely congruent with the Indo-1 Ca^{2+} imaging data demonstrating well-defined tip-directed cytoplasmic Ca^{2+} gradient in wild-type, but not in *Atsfh1* nullizygous, root hairs.

Atsfh1 root hairs fail to properly organize MTs

In addition to the f-actin cytoskeleton, MT networks also function in maintaining polarized tip growth (Bibikova et al., 1999; Baluška et al., 2000; Stevenson et al., 2000; Smith, 2003). MTs appear to consolidate the results of polarized membrane deposition, and MT action in supporting tip growth is spatially regulated by Ca^{2+} gradients (Bibikova et al., 1999; Baluška et al., 2000; Smith, 2003). To assess whether or not the derangements in Ca^{2+} signaling observed in *Atsfh1::T-DNA* root hairs coincided with functional derangement of MT systems, we probed root hair MT organization in AtSfh1p-deficient root hairs by GFP-MAP4 imaging (Marc et al., 1998). As reported by Smith (2003), cortical MTs were organized into discrete filaments. These MT filaments were arranged in spiraling profiles parallel to the longitudinal axis of the cortical plasma membrane in wild-type root hairs (Fig. 8 A and Video 8, available at http://www.jcb.org/cgi/content/full/jcb.200412074/DC1). In contrast, *Atsfh1* root hairs exhibited only diffuse GFP-MAP4 staining profiles (Fig. 8, B and C; and Videos 9 and 10, available at http://www.jcb.org/cgi/content/full/jcb.200412074/DC1). Neither discrete filaments nor obvious spiraling profiles were seen. However, the body of the trichoblast from which the mutant root hair emanates did exhibit organized MTs (Fig. 8 C and Video 10). Thus, *Atsfh* nullizygous root hairs elaborate defects in MT assembly and/or organization that are limited to the growing root hair itself.

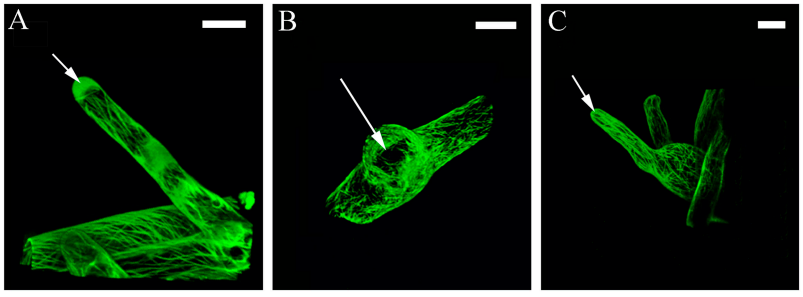

Figure 6. **F-actin imaging in root hairs.** (A) The peripheral actin cables are revealed by talin-GFP imaging as is the fine tip-directed f-actin network (arrow). F-actin imaging in mutant single (B) and double (C) root hairs. Arrows indicate compromise of the fine tip-directed f-actin network. Bars, 20 μm.

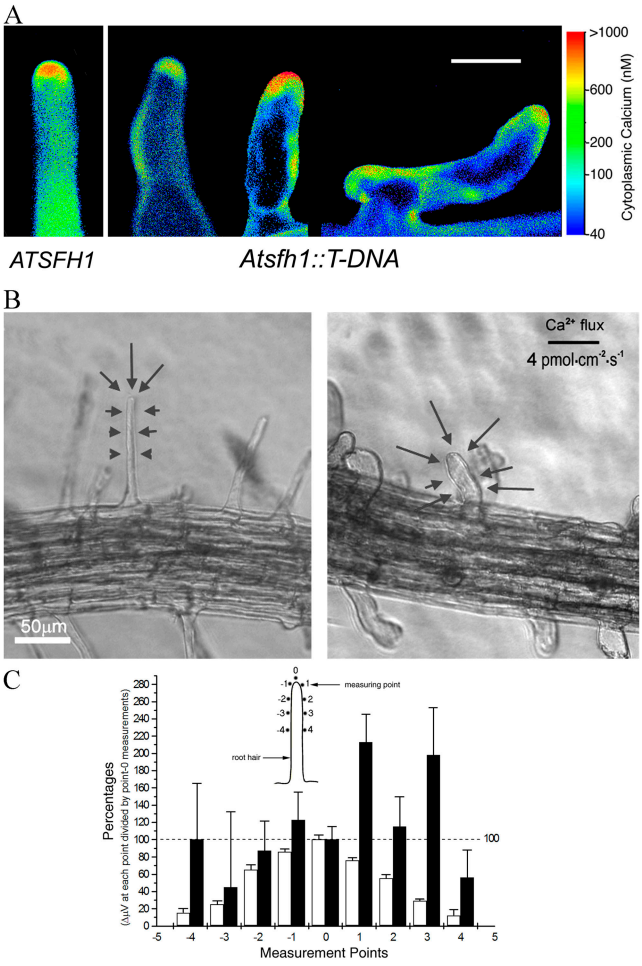

Figure 7. **Defective Ca^{2+} signaling in AtSfh1p-deficient root hairs.** (A) Ca^{2+} gradients. Ca^{2+} concentrations in wild-type (left) and mutant (right) root hairs are in pseudocolor calibrated with the inset scale shown at right. Bar, 25 μm. (B) Typical profile of Ca^{2+} fluxes around the root hairs of both wild-type and *Atsfh1* nullizygous seedlings (3-d-old), as indicated. Measurements were taken at predefined locations, and the Ca^{2+} selective probe was positioned 2 μm away from the root hair surface at those locations. The excursion of the probe is perpendicular to the surface. Arrows show the magnitude and direction of the Ca^{2+} flux at the position on the root hair surface indicated. (C) Ca^{2+} flux profiling of wild-type and *Atsfh1* nullizygous seedlings (3-d-old). The percentages were obtained by dividing the raw Ca^{2+} flux values (ΔμV) measured at each indicated position by the values measured at position 0 (inset). The averages of Ca^{2+} flux values from measurements of 15 independent root hairs are shown with standard errors. Single root hairs of *AtSfh1::T-DNA* plants were used in these analyses.

Discussion

Root hair development requires polarized membrane growth from a precise position on the root epidermal cell plasma membrane. Herein, we demonstrate that loss of AtSfh1p, a PtdCho- and PtdIns-binding/transfer protein with the ability to regulate PIP metabolism, deranges root hair growth. AtSfh1p dysfunction compromises tip-directed plasma membrane PtdIns(4,5)P_2 and Ca^{2+} gradients, elicits tip actin defects, and disorganizes root hair MT networks. The result is a derangement of polarized membrane growth after the site of root hair emergence has been correctly specified. We propose the primary function of AtSfh1p is to generate PIP landmarks that couple to components of the f-actin cytoskeleton, thereby focusing membrane delivery to the root hair tip plasma membrane. The polarized secretory pathway restricts insertion of cargo (e.g., ion channels) to the root hair apex, thereby establishing a tip-directed Ca^{2+} gradient. This gradient cues an organized MT assembly that further reinforces and maintains tip-directed membrane trafficking (Fig. 9).

The data presented emphasize AtSfh1p-mediated regulation of PIP metabolism. What is the mechanism that underlies such regulation? One simple mechanism is that AtSfh1p directly couples its intrinsic AtSfh1p-LBD PtdIns binding/transfer activity to PtdIns kinase action. By this model, AtSfh1p generates PIP signaling pools that regulate the action of multiple effector proteins that couple to actin dynamics and the activities of signaling enzymes (such as PLD). With regard to PLD, an alternative possibility is that AtSfh1p couples its intrinsic PtdCho-binding/transfer activity to PIP synthesis in the plant. In this regard, single or multiple PLD isoforms represent attractive candidates for AtSfh1p effectors. PLDs are PtdIns(4,5)P_2-activated PtdCho hydrolases that generate phosphatidic acid (PtdOH), itself a lipid stimulator of PtdIns-4-phosphate 5-kinase. By presenting PtdCho to PLD, AtSfh1p may initiate a robust positive feedback loop that links PLD activity to PIP synthesis via PtdOH signaling. Obviously, PIP signaling mediated by PtdIns-bound AtSfh1p could cooperate with such a regulatory loop. In support of an AtSfh1p-PLD coupling model, Ohashi et al. (2003) found that PLDζ1 activity regulates root hair growth, and that, like AtSfh1p and PtdIns(4,5)P_2, PLDζ1 is enriched in the tip cytoplasm of growing root hairs. Those results suggest a role for PLDζ1, and perhaps other PLD isoforms, in root hair morphogenesis. A general precedent for a PITP-PLD coupling also exists in yeast, where nonclassical Sec14p-like PITPs function to optimally activate PLD. In that case, PITPs do so by stimulating PIP synthesis in the absence of direct PITP-regulated PtdCho signaling (Xie et al., 1998; Li et al., 2000).

How might AtSfh1p-stimulated PtdIns(4,5)P_2 synthesis interface with the actin cytoskeleton and membrane trafficking? PtdIns(4,5)P_2 synthesis may recruit actin to the Golgi surface and modulate its assembly in a polymerization reaction that potentiates vesicle budding. Evidence for an actin involvement in vesicle formation from mammalian Golgi membranes has been reported (Fucini et al., 2000). However, as neither Golgi morphology nor Golgi distribution is perturbed in *Atsfh1::T-DNA* root hairs, we conclude that the membrane trafficking defects occur at a post-Golgi stage. We speculate AtSfh1p stimulates PLD activity, and ultimately PtdIns(4,5)P_2 synthesis, on formed (or forming) secretory vesicles. Such a regulatory loop promotes an on-demand PtdIns(4,5)P_2-driven actin polymerization on the transport vesicles and engages nascent vesicles with an f-actin pool that imposes polarized trafficking of those post-Golgi vesicles to the root hair tip plasma membrane. It follows that defects in such a lipid signaling program would compromise a specific f-actin component dedicated to vesicle trafficking. The consequence is imposition of kinetic and polarity defects on membrane trafficking to the

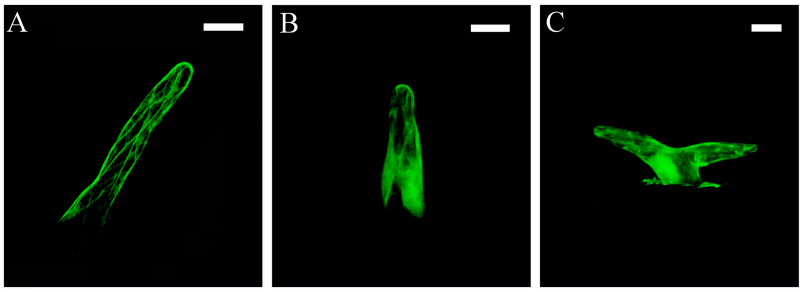

Figure 8. **Defective organization of the MT cytoskeleton in AtSfh1p-deficient root hairs.** (A) MT imaging in wild-type root hairs using MAP4-GFP. The cortical MT network is obvious. MTs in mutant single (B) and double (C) root hairs. *Atsfh1::T-DNA* root hairs fail to construct a defined cortical MT network. Bars, 20 μm.

Atsfh1::T-DNA root hair plasma membrane. GTPases of the Rac/Rho/Cdc42 family, and actin binding proteins (e.g., profilin), are attractive candidates as downstream effectors of AtSfh1p-mediated lipid signaling (Braun et al., 1999; Molendijk et al., 2001). It remains possible, perhaps likely, that AtSfh1p sits at the nexus of more complicated lipid signaling cascades. For example, PtdOH modulates PtdIns 3-OH kinase signaling in polar root tip growth (Anthony et al., 2004).

We further suggest that highly polarized membrane deposition at the root hair plasma membrane of wild-type plants sets the tight Ca^{2+} tip gradient by restricting the distribution of functional Ca^{2+} channels to a focused site on the tip plasma membrane. The net effect is a tip-restricted mode of Ca^{2+} entry into the developing root hair from the extracellular milieu. Our demonstration that nullizygous root hairs engage in precocious and isotropic Ca^{2+} entry across the plasma membrane is consistent with delocalized Ca^{2+} channel distribution. We suggest this is a direct consequence of isotropic fusion of post-Golgi vesicles to the root hair plasma membrane. We also note the observed derangements in Ca^{2+} signaling are not consistent with a role for PtdIns(4,5)P_2-specific phospholipase C–mediated generation of IP_3 in the gating of *Atsfh1* nullizygous root hair plasma membrane Ca^{2+} channels. Were IP_3-gated Ca^{2+} channels involved in generating the cytoplasmic Ca^{2+} gradients, reductions in Ca^{2+} fluxes would have been expected, not the robust and isotropic Ca^{2+} influxes recorded. As the Ca^{2+} tip gradient then cues appropriate organization of the root hair MT cytoskeleton so that polarized membrane delivery to the root hair apex is further reinforced and consolidated (Bibikova et al., 1999), spatial derangement of Ca^{2+} signaling accounts for the lack of organized cortical MT assembly in mutant root hairs.

Herein, we identify AtSfh1p as a key regulator of polarized membrane trafficking in root hairs. A corollary to these findings is that AtSfh1p, or other members of the Sec14p-nodulin domain family, serve as attractive targets for intervention when root hair membrane growth is naturally reoriented, i.e., as occurs in legumes in response to *Rhizobium* NOD factors. The regulation of a Sec14p-nodulin domain protein (LjPLP-IVp) during nodulogenesis in the legume *Lotus japonicus* provides an interesting case in point. LjPLP-IVp is the *Lotus* orthologue of AtSfh1p (Fig. 1, A and B). During nodulation, the promoter driving full-length *LjPLP-IV* transcription is silenced and an internal bidirectional promoter is activated. The result is high level expression, in nodules, of the Nlj16 nodulin and of antisense transcripts directed against the LjPLP-IVp-LBD coding region (Kapranov et al., 2001). We suggest *LjPLP-IV* transcriptional reprogramming during nodulogenesis is designed to efficiently subvert the normal highly polarized root hair growth program by three converging mechanisms that functionally inactivate a master polarity regulator (LjPLP-IVp). First, formation of new transcripts encoding a functional LjPLP-IVp is terminated. Second, production of antisense RNAs directed against the LjPLP-IVp-LBD coding region silence existing full-length LjPLP-IVp transcripts encoding. Third, residual LjPLP-IVp activity is suppressed via high level expression of a dominant-interfering plasma membrane–targeting module that represents the nodulin itself.

Finally, our functional characterization of AtSfh1p raises the intriguing possibility that Sec14p-nodulin domain proteins define a family of polarized membrane growth regulators in plants. We suggest individual members of this family are dedicated to specific polarity establishment events such as those involving organogenesis and control of intracellular organelle

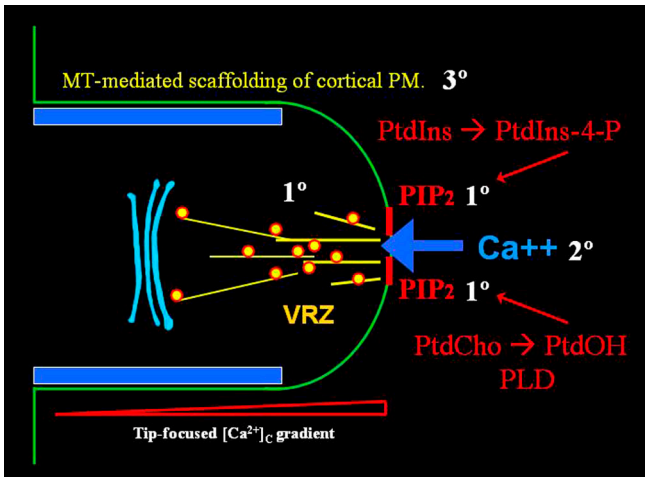

Figure 9. **A model for AtSfh1p-mediated control of polarized membrane growth in developing *A. thaliana* root hairs.** AtSfh1p stimulates PIP synthesis on secretory vesicles and thereby drives f-actin assembly for polarized trafficking to the root hair tip. We propose this PIP synthesis involves a coupling of AtSfh1p with PtdIns kinases or PLD and PtdIns-4-phosphate 5-kinase, or both. Polarized vesicle trafficking generates a tip-directed plasma membrane PtdIns(4,5)P_2 gradient and localized Ca^{2+} influx at the tip plasma membrane, presumably due to tip-restricted insertion of secretory vesicles carrying Ca^{2+} channels. The Ca^{2+} gradient guides spatial organization of cortical MTs in consolidation of tip growth. We posit the primary (1°) defect in *Atsfh1::T-DNA* root hairs is collapse of this PtdIns(4,5)P_2/f-actin control of polarized membrane trafficking. This secondarily (2°) results in isotropic Ca^{2+} influx into the root hair. Disorganization of tip-directed cytoplasmic Ca^{2+} gradients deranges the cortical MT cytoskeleton as a tertiary effect (3°).

morphogenesis. Because the mammalian genome encodes multiple uncharacterized Sec14p domain proteins, Sec14p domain proteins may represent conserved features of lipid-signaling mechanisms that control polarized membrane biogenic programs in eukaryotic cells.

Materials and methods

Bioinformatic methods
Sequences were analyzed by BLAST (http://www.ncbi.nlm.nih.gov/BLAST/ and http://arabidopsis.org/Blast/). Sequence alignments were generated in ClustalX and multiple alignments were shaded with BOXSHADE 3.21 (http://www.ch.embnet.org/software/BOX_form.html).

Yeast strains
Strains included are as follows: CTY182 (*MATa ura3-52 lys2-801 Δhis3-200*), CTY1-1A (CTY182 *sec14-1^{ts}*), CTY1079 (CTY1-1A *spo14Δ::HIS3*), and CTY303 (*MATa ura3-52 lys2-801 Δhis3-200 Δsec14, cki1::HIS3*) (Cleves et al., 1991b; Phillips et al., 1999; Li et al., 2000; Yanagisawa et al., 2002).

Media, genetic techniques, and PIP determinations
Yeast media, genetic techniques, invertase assays, EM, phospholipid transfer assays, and PIP determinations have been described previously (Kearns et al., 1998b; Guo et al., 1999; Phillips et al., 1999; Li et al., 2000; Yanagisawa et al., 2002). Site-directed mutagenesis used QuickChange (Stratagene). Primers were obtained from the University of North Carolina Lineberger Comprehensive Cancer Center Oligonucleotide Synthesis Core.

Plant cDNA isolation
100 μg of total mRNA was prepared from 100 mg of 3-d-old seedlings using the RNeasy Plant Mini Kit (QIAGEN). The 717-bp mRNAs for each *AtSFH-LBD* were amplified for RT-PCR (SuperScript First-Strand Synthesis System; Invitrogen). BamHI and HindIII-restricted cDNAs were cloned into the corresponding sites of a yeast episomal plasmid derived from YEp*lac195* (http://genome-www2.stanford.edu/vectordb/vector_descrip/COMPLETE/YEPLAC195.SEQ.html). *AtSFH-LBD* expression was driven by a *SEC14* promoter and subject to *SEC14* termination signals.

GUS histochemistry
5-d-old seedlings were stained for GUS activity using standard protocols (Jefferson et al., 1987). The *GUS* gene was placed under the control of the *AtSFH1* promoter (P_{AtSFH1}) and transgenic lines were generated by *Agrobacterium*-mediated transformation of wild-type plants using the floral dip method. P_{AtSFH1}::GUS expression was recorded after staining under vacuum for 5 min at 25°C followed by 1 h at 37°C. P_{AtSFH1} represented a 1958-bp DNA fragment directly 5′ to the *AtSFH1* initiator codon.

Imaging and video processing
Light microscopy was done with a microscope (model MZFLIII; Leica) using a cooled CCD camera (model EOSD30; Canon) interfaced with capture image software (RemoteCapture 1.1; Canon), a dissecting microscope (model SMZ-U; Nikon), or a Microphot microscope (Nikon) interfaced with a color CCD camera (model DXM1200; Nikon). Pictures were processed in Photoshop 7.0. Environmental scanning EM (ESEM) used living seedlings mounted in 0.8% (wt/vol) top agar visualized with an ESEM TMP instrument (model XL 30; Philips). Images were processed in Photoshop 7.0. Cytoplasmic Ca^{2+} measurements were performed by microinjecting root cells with Indo-1 conjugated to a 10-kD dextran (Molecular Probes) coupled with confocal ratio imaging (Wymer et al., 1997). GFP-talin and GFP-MAP4 reporters have been described previously (Kost et al., 1998; Bibikova et al., 1999). Confocal and Nomarski microscopy was performed with seedlings mounted in water and covered with number 1.5 coverslips. Fluorescence was scanned with an inverted confocal microscope (model 510 meta; Carl Zeiss MicroImaging, Inc.; 63× C-Apochromat 1.2 NA water immersion lens). GFP experiments used standard FITC settings. For YFP, laser excitation and dichroic filters were set at either 458 or 488 nm, and a 505–530-nm bandpass emission filter was used. The confocal pinhole setting was 1 Airy disk unit and z-stack step size was 0.44 μm. z-Stacks were observed unprocessed. All static images were flattened using an average projection. Volume rendering used Volocity 2 software (Improvision). Plants exhibiting comparable GFP or YFP fluorescence were identified using an inverted fluorescent microscope (model DMIRB; Leica) with standard FITC bandpass filter sets (10 0.3 NA objective). For each experiment, seven independent seedlings were analyzed and <2 root hairs were imaged from each seedling.

Ratiometric imaging
$PH_{PLC\delta1}$–YFP fluorescence was normalized to bulk plasma membrane by dividing intensities of YFP fluorescence (emission bandpass 505–530 nm) by fluorescence of a bulk plasma membrane marker FM 1–43 (Molecular Probes; emission bandpass 530–600 nm) in superimposed images of double-labeled root hairs. Excitation was at 458 nm for both dyes. Endocytosis of FM 1–43 was blocked by pretreating plants with 10 mM NaN_3 for 20 min. Plasma membrane staining was imaged immediately after FM 1–43 (1 μM) was added to bathing medium. The $PH_{PLC\delta1}$–YFP plasmid used in generating the transgenic plants was donated by T. Munnik and W. van Leeuwen (University of Amsterdam, Amsterdam, Netherlands).

EM
3-d-old seedlings were processed for EM essentially as described previously (Čiamporová et al., 2003). Ultrathin sections were observed with an electron microscope (model Tecnai 12; FEI) interfaced with a multiscan camera (model 794; Gatan). All images were processed in Photoshop 7.0.

Plant growth and transformation
Seeds were plated in 0.8% (wt/vol) top agar (low-melt agarose in 1× Murashige and Skoog Salt and Vitamin Mixture media [MS; GIBCO BRL]). Seedlings were stratified at 4°C for 4 d, and then grown vertically under constant light (90 μM m^{-2} s^{-1}) at 22°C for 3 d. Adult roots were extracted after 45 d of growth in soil, cleaned in MS media, and stained either with Ponceau red or Coomassie blue for 30 min. The *Atsfh1::T-DNA* line of *A. thaliana* (Brassica family, Columbia ecotype) was obtained from the Arabidopsis Biological Resource Center via TAIR (http://arabidopsis.org; Alonso et al., 2003). The T-DNA insertion was mapped at the Salk Institute Genomic Analysis Laboratory "T-DNA Express" Arabidopsis Gene Mapping Tool (http://signal.salk.edu/cgi-bin/tdnaexpress). *Atsfh1::T-DNA* mutants were selected for kanamycin resistance (50 μg/ml). Genotypes were confirmed by PCR, Southern blotting, and DNA sequencing of junctional borders. *Agrobacterium tumefaciens*–mediated transformation floral dip protocols were routinely used to generate transgenic plant lines (Clough and Bent, 1998).

Plant material and preparation for SIET
Seeds were incubated for 72 h at 4°C and sterilized in 70% (wt/vol) ethanol for 2 min and 30% (wt/vol) bleach containing 0.01% (wt/vol) Triton X-100 for 25 min. Seeds were placed on sterilized filter paper strips (Fisher Scientific) in Petri dishes (Fisher Scientific) with ∼120 seeds per dish (15 seeds per strip on 8 strips). Approximately 3 ml of sterilized liquid growth media was added to each Petri dish, and dishes were sealed with parafilm and positioned vertically on a rack. Seedlings were germinated in a Pervical growth chamber at 22°C with a 16:8 h light/dark cycle and 68% relative humidity conditions. Growth medium was sterilized before use and was comprised of 0.1 mM KCl, 0.1 mM $CaCl_2$, 0.1 mM $MgCl_2$, 0.5 mM NaCl, 0.3 mM MES, 0.2 mM Na_2SO_4, and 6% sucrose, pH 6.0. Filter paper strips containing three to five seedlings were cut off from the Petri dish and glued to the bottom of a measurement Petri dish. Approximately 5 ml of fresh growth medium was added to the chamber and equilibrated for at least 1 h. To avoid acidification of the medium, media were again replaced and the system allowed to stabilize for 15–20 min before Ca^{2+} flux measurements.

Ca^{2+} flux measurements by SIET
The SIET (Applicable Electronics, Inc.) determines both static ionic/molecular concentrations and concentration gradients by using ion-selective microelectrodes (Kühtreiber and Jaffe, 1990; Schiefelbein et al., 1992). The concentration gradient is measured by moving the electrode repeatedly between two positions in a predefined excursion (5–30 μm) at a fixed frequency in the range of 0.3 to 0.5 Hz. The ion-selective electrode was constructed as follows: glass micropipettes (2 μm aperture) were pulled from 1.5-mm-diam glass capillaries (TW150-4; World Precision Instruments, Inc.) with an electrode puller (P2000; Sutter Instrument Co.) to provide microelectrodes with a 2-μM aperture using a four-step protocol. Micropipettes were silanized with N–N dimethyltrimethylsilamine (Fluka) at 120°C for 50 min, back-filled with 100 mM $CaCl_2$, and then front-filled with Liquid Ion Exchanger (Fluka for Ca^{2+} electrode) to generate the Ca^{2+}-selective probe. The micropipette was placed into an Ag/AgCl wire holder (WPI; reconditioned every time before measurement with self-constructed 9 V DC

circuit). The reference was a solid, low leakage electrode (WPI). Ca^{2+} electrodes were calibrated using a series of 1-, 0.1-, and 0.01-mM $CaCl_2$ solutions. Only electrodes with Nernstian slopes >25 mV were used. Ca^{2+} ion flux was calculated from Fick's law of diffusion: $J = -D(dc/dx)$, where J = ion flux in x direction, dc/dx = ion concentration gradient, and D = ion diffusion constant. Flux direction was determined by electrode movement with respect to sample and sign of calculated flux.

Online supplemental material

Fig. S1 and Video 1 show localization of GFP-AtSfh1p to the plasma membrane and VRZ of wild-type root hairs of 3-d-old transgenic plants. Fig. S2 and Videos 2–4 show YFP-$PH_{PLC\delta1}$ distribution and report the derangement of PtdIns(4,5)P_2 distribution in nullizygous versus wild-type root hairs. Fig. S3 shows Golgi distribution is similar in wild-type and mutant root hairs. Videos 5–7 show GFP-talin imaging in wild-type and nullizygous root hairs and demonstrate loss of the fine tip actin microfilament network in nullizygous root hairs. Videos 8–10 show GFP-MAP4 imaging in root hairs of wild-type and nullizygous root hairs and demonstrate comprehensive loss of organized MTs in nullizygous root hairs. Online supplemental material is available at http://www.jcb.org/cgi/content/full/jcb.200412074/DC1.

We are indebted to Joe Kieber for his invaluable advice, insights, sharing of expertise, and access to technology in his laboratory. We thank Claire Hutchison, Jean Deruere, Alan Jones, Andrew Morris, and Brenda Temple (University of North Carolina, Chapel Hill, NC) for valuable discussions and technical advice; Teun Munnik and Wessel van Leeuwen for the $PH_{PLC\delta1}$–YFP plasmid; John York and June de la Cruz (Duke University, Durham, NC) for access to automated HPLCs for PIP analyses; and Al Shipley (Applicable Electronics, Inc., Forestdale, MA) for critical reading of the manuscript. ESEM was performed at the Duke Biological Sciences EM Facility.

This work was supported by National Institutes of Health grant GM44530 (V.A. Bankaitis) and fellowship "Bourse Lavoisier" from the French Foreign Ministry (P. Vincent). The authors have no conflicting financial interests.

Submitted: 16 December 2004
Accepted: 11 January 2005

References

Alb, J.G., Jr., S.E. Phillips, K. Rostand, L. Cotlin, J. Pinxteren, T. Manning, S. Guo, J.D. York, H. Sontheimer, J.F. Collawn, and V.A. Bankaitis. 2002. Ablation of phosphatidylinositol transfer protein function in murine cells. *Mol. Biol. Cell.* 13:739–754.

Alb, J.G., Jr., J.D. Cortese, S.E. Phillips, R.L. Albin, T.R. Nagy, B.A. Hamilton, and V.A. Bankaitis. 2003. Mice lacking phosphatidylinositol transfer protein alpha exhibit spinocerebellar degeneration, intestinal and hepatic steatosis, and hypoglycemia. *J. Biol. Chem.* 278:33501–33518.

Alonso, J.M., A.N. Stepanova, T.J. Leisse, C.J. Kim, H. Chen, P. Shinn, D.K. Stevenson, J. Zimmerman, P. Barajas, R. Cheuk, et al. 2003. Genome-wide insertional mutagenesis of *Arabidopsis thaliana*. *Science*. 301:653–657.

Anthony, R.G., R. Henriques, A. Helfer, T. Meszaros, G. Rios, C. Testerink, T. Munnik, M. Deak, C. Koncz, and L. Borge. 2004. A protein kinase target of a PDK1 signalling pathway is involved in root hair growth in *Arabidopsis*. *EMBO J.* 23:572–581.

Baluška, F., J. Salaj, J. Mathur, M. Braun, F. Jasper, J. Šamaj, N.-H. Chua, P.W. Barlow, and D. Volkmann. 2000. Root hair formation: f-actin-dependent tip growth is initiated by local assembly of profilin-supported f-actin meshworks accumulated within expansin-enriched bulges. *Dev. Biol.* 227:618–632.

Bankaitis, V.A., J.R. Aitken, A.E. Cleves, and W. Dowhan. 1990. An essential role for a phospholipid transfer protein in yeast Golgi function. *Nature.* 347:561–562.

Bankaitis, V.A., J. Cortese, S.E. Phillips, and J.G. Alb Jr. 2004. Phosphatidylinositol transfer protein function in the mouse. *Adv. Enzyme Regul.* 44:201–218.

Bibikova, T.N., E.B. Blancaflor, and S. Gilroy. 1999. MTs regulate tip growth and orientation in root hairs of *Arabidopsis thaliana*. *Plant J.* 17:657–665.

Braun, M., F. Baluška, M. von Witsch, and D. Menzel. 1999. Redistribution of actin, profilin and phosphatidylinositol-4,5-bisphosphate in growing and maturing root hairs. *Planta.* 209:435–443.

Čiamporová, M., K. Dekánková, Z. Hanáčkova, P. Peters, M. Ovečaka, and F. Baluška. 2003. Structural aspects of bulge formation during root hair initiation. *Plant Soil.* 255:1–7.

Cleves, A.E., T.P. McGee, and V.A. Bankaitis. 1991a. Phospholipid transfer proteins: a biological debut. *Trends Cell Biol.* 1:30–34.

Cleves, A.E., T.P. McGee, E.A. Whitters, K.M. Champion, J.R. Aitken, W. Dowhan, M. Goebl, and V.A. Bankaitis. 1991b. Mutations in the CDP-choline pathway for phospholipid biosynthesis bypass the requirement for an essential phospholipid transfer protein. *Cell.* 64:789–800.

Clough, S.J., and A.F. Bent. 1998. Floral dip: A simplified method for *Agrobacterium*-mediated transformation of *Arabidopsis thaliana. Plant J.* 16:735–743.

Fang, M., A. Gedvilaite, B.G. Kearns, S. Kagiwada, M. Kearns, M.K.Y. Fung, and V.A. Bankaitis. 1996. Kes1p shares homology with human oxysterol binding protein homolog and participates in a novel regulatory pathway for yeast Golgi-derived secretory vesicle biogenesis. *EMBO J.* 15:6447–6459.

Fucini, R.V., A. Navarette, C. Vadakkan, L. Lacomis, H. Erdjument-Bromage, P. Tempst, and M. Stamnes. 2000. Activated ADP-ribosylation factor assembles distinct pools of actin on Golgi membranes. *J. Biol. Chem.* 275:18824–18829.

Guo, S., L.E. Stolz, S. Lemrow, and J.D. York. 1999. *SAC1*-like domains of yeast *SAC1, INP52* and *INP53*, and human synaptojanin encode polyPIP phosphatases. *J. Biol. Chem.* 274:12990–12995.

Jefferson, R.A., T.A. Kavanagh, and M.W. Bevan. 1987. GUS fusions: β-glucuronidase as a sensitive and versatile gene fusion marker in higher plants. *EMBO J.* 6:3901–3907.

Jones, B., E.L. Jones, S.A. Bonney, H.N. Patel, A.R. Mensenkamp, S. Eichenbaum-Voline, M. Rudling, U. Myrdal, G. Annesi, S. Naik, et al. 2003. Mutations in a Sar1 GTPase of COPII vesicles are associated with lipid absorption disorders. *Nat. Genet.* 34:29–31.

Jouannic, N., M. Lepetit, C. Vergnolle, C. Cantrel, A.M. Gardies, J.C. Kader, and V. Arondel. 1998. Isolation of a cDNA from *Arabidopsis thaliana* that complements the *sec14* mutant of yeast. *Eur. J. Biochem.* 258:402–410.

Kapranov, P., S.M. Routt, V.A. Bankaitis, F.J. de Bruijn, and K. Szczyglowski. 2001. Novel developmental regulation of phosphatidylinositol transfer protein expression in nitrogen-fixing root nodules of the flowering plant *Lotus japonicus. Plant Cell.* 13:1369–1382.

Kearns, B.G., J.G. Alb Jr., and V.A. Bankaitis. 1998a. Phosphatidylinositol transfer proteins: the long and winding road to function. *Trends Cell Biol.* 8:276–282.

Kearns, M.A., D.E. Monks, M. Fang, M.P. Rivas, P.D. Courtney, J. Chen, G.D. Prestwich, A.B. Theibert, R.E. Dewey, and V.A. Bankaitis. 1998b. Novel developmentally regulated PIP binding proteins from soybean whose expression bypasses the requirement for an essential phosphatidylinositol transfer protein in yeast. *EMBO J.* 17:4004–4017.

Ketelaar, T., N.C. de Ruitjer, and A.M. Emons. 2003. Unstable F-actin specifies the area and MT direction of cell expansion in *Arabidopsis* root hairs. *Plant Cell.* 15:285–292.

Kost, B., P. Spielhofer, and N.-H. Chua. 1998. A GFP-mouse talin fusion protein labels plant actin filaments in vivo and visualizes the actin cytoskeleton in growing pollen tubes. *Plant J.* 16:393–401.

Kühtreiber, W.M., and L.F. Jaffe. 1990. Detection of extracellular calcium gradients with a calcium-specific vibrating electrode. *J. Cell Biol.* 110:1565–1573.

Li, X., S. Routt, Z. Xie, X. Cui, M. Fang, M.A. Kearns, M. Bard, D. Kirsch, and V.A. Bankaitis. 2000. Identification of a novel family of nonclassical yeast PITPs whose function modulates activation of PLD and Sec14p-independent cell growth. *Mol. Biol. Cell.* 11:1989–2005.

Li, X., M.P. Rivas, M. Fang, J. Marchena, B. Mehrotra, A. Chaudhary, L. Feng, G.D. Prestwich, and V.A. Bankaitis. 2002. Analysis of oxysterol binding protein homologue Kes1p function in regulation of Sec14p-dependent protein transport from the yeast Golgi complex. *J. Cell Biol.* 157:63–77.

Marc, J., C.L. Granger, J. Brincat, D.D. Fisher, T.-H. Kao, A.G. McCubbin, and R.J. Cyr. 1998. A GFP-MAP4 reporter gene for visualizing cortical MT rearrangements in living epidermal cells. *Plant Cell.* 10:1927–1939.

Mathur, J., and M. Hülskamp. 2002. Microtubules and microfilaments in cell morphogenesis in higher plants. *Curr. Biol.* 12:R669–R676.

Molendijk, A.J., F. Bischoff, C.S.V. Rajendrakumar, J. Friml, M. Braun, S. Gilroy, and K. Palme. 2001. *Arabidopsis thaliana* Rop GTPases are localized to tips of root hairs and control polar growth. *EMBO J.* 20:2779–2788.

Ohashi, Y., A. Oka, R. Rodrigues-Pousada, M. Possenti, I. Ruberti, G. Morelli, and T. Aoyama. 2003. Modulation of phospholipid signaling by GLABRA2 in root hair pattern formation. *Science.* 300:1427–1430.

Phillips, S., B. Sha, L. Topalof, Z. Xie, J. Alb, V. Clenchin, P. Swigart, S. Cockcroft, M. Luo, T. Martin, and V. Bankaitis. 1999. Yeast Sec14p deficient in phosphatidylinositol transfer activity is functional in vivo. *Mol. Cell.* 4:187–197.

Routt, S.M., and V.A. Bankaitis. 2004. Biological functions of phosphatidylinositol transfer proteins. *Biochem. Cell Biol.* 82:254–262.

Schiefelbein, J.W., A. Shipley, and P. Rowse. 1992. Calcium influx at the tip of growing root hair cells of *Arabidopsis thaliana*. *Planta.* 187:455–459.

Sha, B., S.E. Phillips, V.A. Bankaitis, and M. Luo. 1998. Crystal structure of the *Saccharomyces cerevisiae* phosphatidylinositol-transfer protein. *Nature.* 391:506–510.

Smith, L.G. 2003. Cytoskeletal control of plant cell shape: getting the fine points. *Curr. Op. Plant Biol.* 6:63–73.

Stevenson, J.M., I.Y. Perera, I. Heilmann, S. Persson, and W.F. Boss. 2000. Inositol signaling and plant growth. *Trends Plant Sci.* 5:252–258.

Szczyglowski, K., D. Hamburger, P. Kapranov, and F.J. de Bruijn. 1997. Construction of a *Lotus japonicus* late nodulin expressed sequence tag library and identification of novel nodule-specific genes. *Plant Physiol.* 114:1335–1346.

Wymer, C.L., T.N. Bibikova, and S. Gilroy. 1997. Cytoplasmic free calcium distributions during the development of root hairs of *Arabidopsis thaliana. Plant J.* 12:427–439.

Xie, Z., M. Fang, M.P. Rivas, A. Faulkner, P.C. Sternweis, J. Engebrecht, and V.A. Bankaitis. 1998. Phospholipase D activity is required for suppression of yeast phosphatidylinositol transfer protein defects. *Proc. Natl. Acad. Sci. USA.* 95:12346–12351.

Yanagisawa, L., J. Marchena, Z. Xie, X. Li, P.P. Poon, R. Singer, G. Johnston, P.A. Randazzo, and V.A. Bankaitis. 2002. Activity of specific lipid-regulated ARFGAPs is required for Sec14p-dependent Golgi secretory function in yeast. *Mol. Biol. Cell.* 13:2193–2206.

Yoder, M.D., L.M. Thomas, J.M. Tremblay, R.L. Oliver, L.R. Yarbrough, and G.M. Helmkamp Jr. 2001. Structure of a multifunctional protein. Mammalian phosphatidylinositol transfer protein complexed with phosphatidylcholine. *J. Biol. Chem.* 276:9246–9252.